VOLUME 30 NUMBER 4 October 2024
pISSN 2287-2728
eISSN 2387-285X

CLINICAL and MOLECULAR HEPATOLOGY

The forum for latest knowledge of hepatobiliary diseases

T-cell therapy for HBV-HCC

Mortality from HCC and biliary tract cancers
Liver fibrosis scores and viral load in CHB
Genomic biomarkers for atezolizumab+bevacizumab in HCC
Epigenetic alteration of complement genes in MASLD

KASL

pISSN 2287-2728
eISSN 2287-285X

CLINICAL and MOLECULAR HEPATOLOGY

https://doi.org/10.3350/cmh.2024.0296
Clinical and Molecular Hepatology 2024;30:914-928

Original Article

Development and validation of a stromal-immune signature to predict prognosis in intrahepatic cholangiocarcinoma

Yu-Hang Ye[1,2,*], Hao-Yang Xin[1,2,*], Jia-Li Li[3,*], Ning Li[2], Si-Yuan Pan[1,2], Long Chen[1,2], Jing-Yue Pan[2], Zhi-Qiang Hu[1,2], Peng-Cheng Wang[1,2], Chu-Bin Luo[1,2], Rong-Qi Sun[1,2], Jia Fan[1,2], Jian Zhou[1,2], Zheng-Jun Zhou[2], and Shao-Lai Zhou[1,2]

[1]Department of Liver Surgery and Transplantation, Zhongshan Hospital, Fudan University, Shanghai; [2]Liver Cancer Institute, Zhongshan Hospital, Fudan University, Shanghai; [3]Department of Pathology, Zhongshan Hospital, Fudan University, Shanghai, China

Graphical Abstract

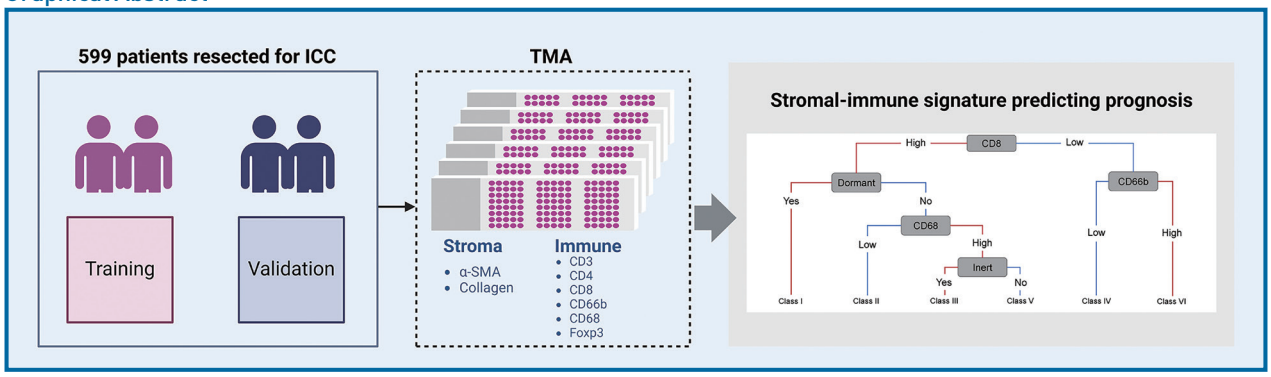

Study Highlights

- Four major patterns of ICC stroma composition according to the distributions of α-SMA and collagen: dormant (α-SMA^{low}/collagen^{high}), fibrogenic (α-SMA^{high}/collagen^{high}), inert (α-SMA^{low}/collagen^{low}), and fibrolytic (α-SMA^{high}/collagen^{low}) were defined. The types of stroma differed from the distributions of α-SMA and collagen and displayed distinct patterns of immune cells, which were predictive of patient prognosis. An integrated stromal-immune signature to predict prognosis in surgically treated ICC was developed and validated.

Backgrounds/Aims: Intrahepatic cholangiocarcinoma (ICC) is a highly desmoplastic tumor with poor prognosis even after curative resection. We investigated the associations between the composition of the ICC stroma and immune cell infiltration and aimed to develop a stromal-immune signature to predict prognosis in surgically treated ICC.

Methods: We recruited 359 ICC patients and performed immunohistochemistry to detect α-smooth muscle actin (α-SMA), CD3, CD4, CD8, Foxp3, CD68, and CD66b. Aniline was used to stain collagen deposition. Survival analyses were performed to detect prognostic values of these markers. Recursive partitioning for a discrete-time survival tree was applied to define a stromal-immune signature with distinct prognostic value. We delineated an integrated stromal-immune signature based on immune cell subpopulations and stromal composition to distinguish subgroups with different recurrence-free survival (RFS) and overall survival (OS) time.

Results: We defined four major patterns of ICC stroma composition according to the distributions of α-SMA and collagen: dormant (α-SMA^{low}/collagen^{high}), fibrogenic (α-SMA^{high}/collagen^{high}), inert (α-SMA^{low}/collagen^{low}), and fibrolytic (α-SMA^{high}/collagen^{low}). The stroma types were characterized by distinct patterns of infiltration by immune cells. We divided patients into six classes. Class I, characterized by high CD8 expression and dormant stroma, displayed the longest RFS and OS, whereas Class VI, characterized by low CD8 expression and high CD66b expression, displayed the shortest RFS and OS. The integrated stromal-immune signature was consolidated in a validation cohort.

Conclusions: We developed and validated a stromal-immune signature to predict prognosis in surgically treated ICC. These findings provide new insights into the stromal-immune response to ICC. **(Clin Mol Hepatol 2024;30:914-928)**

Keywords: Intrahepatic cholangiocarcinoma; Stromal signature; Immune cell; Prognosis

INTRODUCTION

Intrahepatic cholangiocarcinoma (ICC) is the second-most frequent type of primary liver cancer, with an increasing global incidence in recent decades.[1] Radical resection is the best approach to achieve long-term survival; however, only 30–40% of ICC patients are suitable for radical resection, and recurrence rates after surgery remain high, ranging from 40% to 80%.[1,2] The GEMOX regimen, which combines gemcitabine and cisplatin, appears to be the standard therapy for patients with locally advanced ICC, but this treatment is not curative and at best provides only a modest increase in overall survival (OS).

ICC typically exhibits a prominent desmoplastic reaction characterized by dense collagen type 1 fiber deposition and the presence of α-smooth muscle actin (α-SMA)-positive cancer-associated fibroblasts (CAFs). Varying degrees of infiltration by immune cells; such as tumor-associated macrophages (TAMs), tumor-associated neutrophils (TANs), and various types of T-lymphocytes, including T helper cells (CD4+ T cells), cytotoxic T cells (CD8+ T cells), and regulatory T cells (Tregs); are also common in the desmoplastic stroma of ICC.[3] The immune cells infiltrating the tumor microenvironment have been demonstrated to have great significance for ICC development and progression, as well as recurrence and survival in patients with ICC.[4-6] Recent studies convincingly demonstrate the active and crucial role of the desmoplastic reaction in promoting progressive ICC invasive growth and metastasis, cholangiocarcinoma cell survival, resistance to chemotherapy and targeted therapies, and immunosuppression.[7]

Tumor-infiltrating leukocytes that accompany the desmoplastic reaction in ICC are considered to be associated with patient outcomes[8,9]; however, the complexity and plasticity of stroma formation in ICC, as well as the associations of the ICC stroma with immune cells, are largely un-

Corresponding author : Shao-Lai Zhou
Department of Liver Surgery and Transplantation, Liver Cancer Institute, Zhongshan Hospital, Fudan University, 1609 Xie Tu Road, Shanghai 200032, China
Tel: +86-21-64041990, Fax: +86-21-64037181, E-mail: zhoushaolai99@sina.com
https://orcid.org/0000-0002-8526-5221

*These authors contributed equally to this work.

Editor: Ju Dong Yang, Cedars-Sinai Medical Center, USA

Received : Apr. 25, 2024 / **Revised :** Aug. 3, 2024 / **Accepted :** Aug. 5, 2024

Abbreviations:

ICC, intrahepatic cholangiocarcinoma; OS, overall survival; α-SMA, α-smooth muscle actin; CAFs, cancer-associated fibroblasts; TAMs, tumor-associated macrophages; TANs, tumor-associated neutrophils; TNM, tumor-node-metastasis; RFS, recurrence-free survival; TMAs, tissue microarrays; HR, hazard ratio; PI, prognostic index; MDSCs, myeloid-derived suppressor cells; FAP, fibroblast activation protein

known. Therefore, to generate a prognostic landscape of stromal composition and infiltrating leukocytes across ICC, we investigated the stromal composition and infiltration by T-lymphocytes (CD3, CD4, CD8, Foxp3), TAMs, and TANs and developed a novel stromal-immune signature to stratify patients after curative surgery.

MATERIALS AND METHODS

Patients and follow-up

A total of 599 patients with primary ICC who received radical resection from 2009 to 2016 in the Department of Liver Surgical Oncology of Zhongshan Hospital Fudan University were enrolled in the study. One cohort of 359 patients was included from January 2009 to December 2014 for training purposes, and another cohort of 240 patients was included from January 2015 to December 2016 for validation purposes (Supplementary Table 1). Patients who received palliative surgeries or prior interventions (such as trans-hepatic artery embolization, chemotherapy, or radiotherapy) or with other primary malignancies or inflammatory diseases were excluded from the study. Radical resection was defined as complete resection of tumor nodules, with cancer-free tumor margins shown by histologic examination and resection of regional lymph nodes, including the hilar, hepatoduodenal ligament, and caval lymph nodes, with no cancerous thrombus in the portal vein (main trunk or major branches), hepatic veins, or bile duct.[10] Patients with further lymph node involvement were considered to have distant metastasis and were excluded from the study. Histopathological diagnoses were according to World Health Organization criteria, and tumor differentiation grading was according to the classification by Edmondson and Steiner.[11] The Child-Pugh scoring system was applied to assess liver function, and tumor-node-metastasis (TNM) grading was used to define tumor stage according to the 2017 International Union Against Cancer.[12] Patients participating in the study provided informed consent, and the study was approved by the Research Ethics Committee of Zhongshan Hospital.

The patients were monitored after surgery as previously described.[13] The duration from the time of the surgery until death or last observation (December 2018) was used to determine OS. The data from surviving patients were censored at the final follow-up. The duration from the time of surgery to the date on which intrahepatic recurrence or extrahepatic metastasis was diagnosed was used to determine recurrence-free survival (RFS).[14]

Tissue microarray and immunohistochemistry

Tissue microarrays (TMAs) were performed for all 359 cases in cohort 1 and all 240 cases in cohort 2. The paraffin blocks contained areas devoid of necrotic and hemorrhagic damage that were identified in hematoxylin and eosin-stained sections and two 2-mm-diameter biopsy cores containing intratumoral and nontumoral tissues.

Sections from the tissue blocks were rehydrated and subjected to microwave antigen retrieval. Next, the sections were incubated overnight at 4°C with monoclonal antibodies against α-SMA (1:100, clone 1A4; Abcam, Cambridge, UK), CD3 (1:50, clone F7.2.38; DakoCytomation, Glostrup, Denmark), CD4 (1:100, clone EPR6855; Epitomics, Burlingame, CA, USA), CD8 (1:50, clone C8/144B; DakoCytomation), Foxp3 (1:100, clone 236A/E7; Abcam), CD68 (1:200, clone KP1; Abcam), and CD66b (1:500, clone G10F5; BD Biosciences, San Jose, CA, USA), followed by incubation for 30 min at 37°C with secondary antibodies (GK500705; Gene Tech, Shanghai, China). Immunoreactivity was visualized with 3,3'-diaminobenzidine according to the avidin-biotin-peroxidase complex method,[14] followed by counterstaining with Mayer's hematoxylin. Slides in which the primary antibody was omitted served as negative controls. Collagen staining was performed with the collagen-specific aniline blue of the Masson trichrome stain without application of hematoxylin or Biebrich scarlet acid fuchsin as counterstains.

Evaluation of immunohistochemical variables

Three pathologists who were blind to the characteristics of the patients each assessed the immunohistochemical staining, with any discrepancies among their findings resolved by consensus. For the CD3, CD4, CD8, Foxp3, CD68, and CD66b staining in TMAs, the mean numbers of cells with positive immunostaining in triplicate sections were determined (cells/mm^2). Collagen and α-SMA expression in TMAs were determined using Image-Pro Plus v6.2

https://doi.org/10.3350/cmh.2024.0296

software (Media Cybernetics, Inc., Bethesda, MD, USA). The integrated optical density of all positive α-SMA and collagen staining in each photograph was measured, and its ratio to the total area of each photograph was calculated as the α-SMA or collagen density. In subsequent analyses, the median values were used as the cut-offs for high and low expression of α-SMA and collagen. For CD3, CD4, CD8, Foxp3, CD68, and CD66b, the best cut-off values were defined using X-tile.[15] The stromal type in terms of α-SMA/collagen expression was determined as dormant (low α-SMA/high collagen), inert (low α-SMA/low collagen), fibrogenic (high α-SMA/high collagen), or fibrolytic (high α-SMA/low collagen), as described previously.[9]

Defining an immune-stromal signature

An immune-stromal signature consisting of tumor-infiltrating leukocytes and stroma type was generated by non-parametric recursive partitioning for discrete-time survival tree analysis using the R package "rpart". To select the crucial variables, we performed a random survival forest analysis using the R package "randomForestSRC" and assessed the variable of importance (VIMP) and minimal depth (MD). Variables with high VIMP and low MD were considered to contribute to the model.

Statistical analysis

Statistical analyses were performed with R (4.1.1) statistical software. Chi-square and Fisher's exact tests were used to assess associations between clinicopathologic features and immunohistochemistry results as appropriate. For comparison of multiple groups, the Kruskal–Wallis test was performed for continuous variables using the R package "aigicolae", and the Chi-square test was performed for categorical variables using the R package "rcompanion". The Kaplan–Meier method was used to determine RFS and OS, which were analyzed by log-rank test. Pairwise analyses of OS and RFS with Bonferroni adjustment were performed using the R package "survminer". Cox proportional hazards regression was used for univariate and multivariable analyses. All pairwise comparisons were adjusted by the Bonferroni method. *P*-values <0.05 were considered statistically significant.

RESULTS

The stromal composition of ICC and its association with patient outcomes

Among the 359 patients in the training cohort, the mean (standard deviation) age was 58.5 (10.1) years, 206 (57.4%) were male, 187 (52.1%) presented an elevated CA19-9 level (>36), and over half (182 patients) were diagnosed with TNM I stage disease. Representative images of the four types of ICC stromal composition based on the expression of α-SMA and collagen are shown in Figure 1A. Analysis of patient outcomes with respect to the stromal composition showed that higher α-SMA expression was associated with shorter RFS and OS, whereas higher collagen expression was associated with better prognosis (Fig. 1B). The median RFS and OS were 39.60 months (95% confidence interval [CI] 16.20~ months) and 79.70 months (95% CI 41.40~ months) for patients with dormant stroma, 14.20 months (95% CI 9.40–20.40 months) and 23.80 months (95% CI 14.20–38.50 months) for patients with fibrogenic stroma, 13.90 months (95% CI 9.90–20.90 months) and 20.90 months (95% CI 14.40–30.40 months) for patients with inert stroma, and 8.50 months (95% CI 6.60–10.80 months) and 20.30 months (95% CI 12.30–26.80 months) for patients with fibrolytic stroma. Patients with dormant stroma displayed the longest RFS and OS, whereas patients with fibrolytic stroma displayed the shortest RFS and OS. The hazard ratio (HR) for fibrolytic stroma in comparison with dormant stroma was 2.35 (95% CI 1.59–3.49) for RFS and 2.77 (95% CI 1.81–4.22) for OS. Patients with fibrogenic stroma or inert stroma had a worse prognosis than patients with dormant stroma and a better prognosis than patients with fibrolytic stroma (Fig. 1).

To compare the clinicopathological characteristics of the four stroma subtypes, we performed Chi-square tests and found that tumor size and tumor number were associated with the stromal types (Supplementary Table 2). We also performed a multivariable Cox proportional regression analysis of prognostic clinicopathological characteristics and stromal type. We found the stromal type was an independent risk factor for RFS and OS (Table 1). Overall, the stromal type based on differential α-SMA and collagen expression was an important histological characteristic and prognostic factor in ICC.

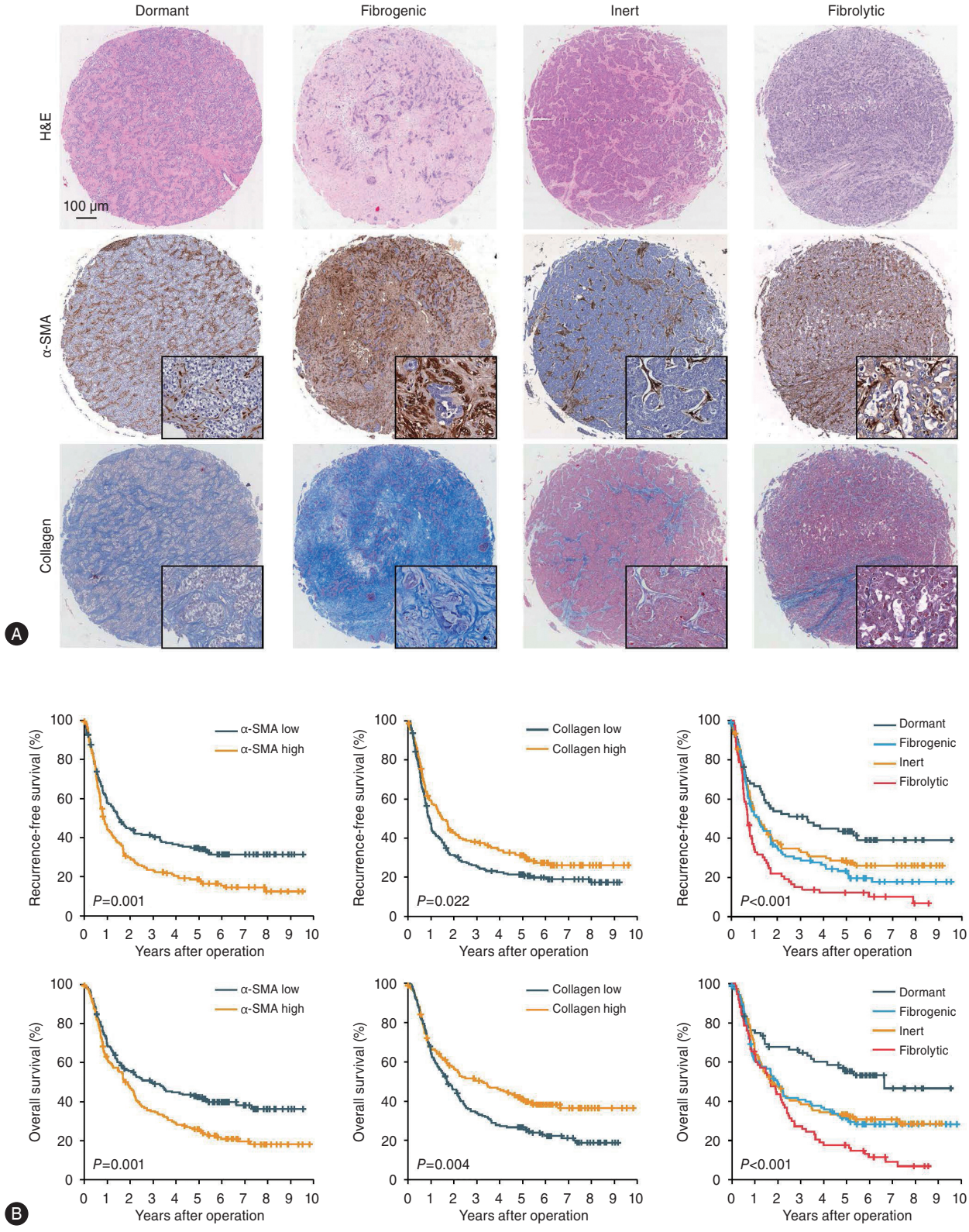

Figure 1. Tumor stromal composition is associated with prognosis in ICC. (A) Stromal composition of different stromal types. (B) K-M curves of RFS and OS among stromal composition and different stromal types. ICC, intrahepatic cholangiocarcinoma; RFS, recurrence-free survival; OS, overall survival; α-SMA, α-smooth muscle actin.

https://doi.org/10.3350/cmh.2024.0296

The composition of immune infiltration and its prognostic association

The number of immune cells infiltrating the tumor microenvironment was previously shown to be associated with recurrence in ICC.[4] Therefore, we quantified CD3+, CD4+, CD8+, Foxp3+, CD68+, and CD66b+ tumor-infiltrating leukocytes in the TMAs by immunohistochemistry and investigated their prognostic associations. To investigate the prognostic significance of the tumor-infiltrating immune cells, we performed Kaplan–Meier survival analyses separately. CD3+, CD4+, and CD8+ T cells are the major effector cells in anti-cancer immunity. High CD3 expression was associated with longer median RFS (19.50 months, 95% CI 14.20–26.20 months) compared with low CD3 expression (8.70 months, 95% CI 7.10–11.80 months; Table 2), resulting in an HR of 0.62 (95% CI 0.49–0.79; *P*<0.001; Table 3). Patients with high CD4 expression also displayed a longer median RFS (38.90 months, 95% CI 34.40–43.40 months) compared with patients with low CD4 expression (median RFS 15.70 months, 95% CI 11.20–20.20 months; Table 2), with an HR of 0.59 (95% CI 0.44–0.79; *P*<0.001; Table 3). In line with CD3 and CD4 expression, high CD8 expression resulted in a favorable median RFS (20.20 months, 95% CI 12.90–30.10 months) compared with low CD8 expression (9.70 months, 95% CI 8.10–13.50 months; Table 2), with an HR of 0.61 (95% CI 0.48–0.77; *P*<0.001; Table 3). Kaplan–Meier analysis of OS and CD3, CD4, and CD8 expression showed similar results (Tables 2 and 3).

In our analysis, Foxp3+ regulatory T cells were not correlated with RFS but displayed a correlation with OS, with median OS of 20.10 months (95% CI 11.80–26.90 months) for patients with high Foxp3 expression and 27.00 months (95% CI 21.50–38.50 months) for patients with low Foxp3 expression, resulting in an HR of 1.32 (95% CI 1.01–1.72; *P*=0.044; Tables 2 and 3).

Table 1. Multivariable Cox analysis of clinicopathological characteristics and stroma types for RFS and OS (n=359)

Characteristics		Recurrence-free survival			Overall survival		
		HR (95% CI)	z score	*P*-value	HR (95% CI)	z score	*P*-value
CA19-9, U/L	≤36	1 (referent)			1 (referent)		
	>36	1.20 (0.92 to 1.56)	1.32	0.185	1.50 (1.13 to 1.98)	2.82	0.005
GGT, U/L	≤54	1 (referent)			1 (referent)		
	>54	1.36 (1.04 to 1.76)	2.29	0.022	1.45 (1.11 to 1.91)	2.69	0.007
HBsAg	Negative	1 (referent)			1 (referent)		
	Positive	1.01 (0.78 to 1.32)	0.11	0.910	0.74 (0.55 to 1.00)	–1.96	0.050
Tumor size, cm	≤5	1 (referent)			1 (referent)		
	>5	1.27 (0.98 to 1.65)	1.84	0.066	1.20 (0.91 to 1.58)	1.27	0.204
Tumor number	Single	1 (referent)			1 (referent)		
	Multiple	1.99 (1.52 to 2.62)	4.95	<0.001	2.21 (1.67 to 2.92)	5.58	<0.001
Lymphatic metastasis	No	1 (referent)			1 (referent)		
	Yes	1.74 (1.26 to 2.39)	3.40	0.001	1.96 (1.40 to 2.73)	3.93	0.001
LVI	No	1 (referent)			1 (referent)		
	Yes	1.25 (0.93 to 1.67)	1.47	0.140	1.35 (0.98 to 1.84)	1.86	0.063
Tumor encapsulation	Complete	1 (referent)			1 (referent)		
	None	1.37 (0.96 to 1.95)	1.74	0.082	1.32 (0.90 to 1.93)	1.43	0.151
Tumor differentiation	I+II	1 (referent)			1 (referent)		
	III+IV	1.25 (0.97 to 1.59)	1.75	0.081	1.31 (1.01 to 1.70)	2.01	0.045
Stroma	Dormant	1 (referent)			1 (referent)		
	Fibrogenic	1.45 (1.00 to 2.12)	1.93	0.053	1.58 (1.04 to 2.40)	2.15	0.032
	Inert	1.29 (0.88 to 1.88)	1.29	0.198	1.48 (0.97 to 2.25)	1.83	0.067
	Fibrolytic	1.94 (1.31 to 2.89)	3.27	0.001	2.11 (1.37 to 3.24)	3.41	0.001

CI, confidence interval; GGT, gamma glutamyl transferase; CA 19-9, carbohydrate antigen 19-9; LVI, lymphatic vascular invasion.

We performed Kaplan–Meier survival analyses based on CD68 and CD66b expression and found that high CD68 or CD66b expression was associated with decreased RFS (Table 2). The median RFS of patients with high CD68 expression was 9.70 months (95% CI 8.40–12.90 months), which was significantly shorter than the median RFS of patients with low CD68 expression (16.30 months, 95% CI 12.00–20.40 months; HR 1.30; 95% CI 1.02–1.66; *P*=0.033; Tables 2 and 3). Likewise, the median RFS of patients with high CD66b expression was 6.10 months (95% CI 5.10–9.60 months), which was significantly shorter than the median RFS of patients with low CD66b expression (15.70 months, 95% CI 11.80–20.20 months; HR 1.75 95% CI 1.28–2.39; *P*<0.001; Tables 2 and 3). We also observed similar effects of CD68 and CD66b expression on OS (Tables 2 and 3). In summary, the composition of immune infiltration had significant associations with patient prognosis.

Connection between the stroma type and immune infiltration

The impact of the stroma on immune cell immigration coordinates the hierarchal interactions between immune cells and tumor cells.[9,15] To identify the association between stromal composition and immune infiltration, we compared the distributions of tumor-infiltrating leukocytes among the different stroma types using the Kruskal–Wallis test with Bonferroni adjustment. We found that the distributions of tumor-infiltrating leukocytes differed among the different stromal subtypes (Fig. 2A). Fibrogenic stroma was characterized by abundant Foxp3+ cells; inert stroma displayed a pattern of abundant CD68+ cells and CD66b+ cells; and fibrolytic stroma had abundant CD3+ cells, CD68+ cells, and CD66b+ cells. There were fewer infiltrating leukocytes in dormant stroma (Fig. 2A), suggesting an inactivated status of immune infiltration.

To identify the interactive effects of tumor-infiltrating leukocytes between different stromal subtypes, we performed a comparative correlation analysis (Fig. 2B). Two clusters of CD3+, CD4+, CD8+, Foxp3+ cells and CD68+, CD66b+ cells were attributed to dormant stroma. Inert stroma showed two dominant clusters of CD3+, CD4+, CD8+, CD68+ cells and Foxp3+, CD66b+ cells. CD3+, CD4+, CD8+ cells and Foxp3+, CD68+, CD66b+ cells were identified as the two main clusters in both fibrogenic stroma and fibrolytic stroma. The results showed that T cells including CD3+, CD4+, and CD8+ were the main cluster of all stroma types.

Because the immune cells showed differential distributions and interactions with respect to stromal types, we tested the influence of different immune cells on prognosis

Table 2. Kaplan–Meier analysis depicts the influences of differential expressions of immune infiltrate markers in predicting RFS and OS (n=359)

Immune markers	Stratification	RFS			OS		
		mRFS (95% CI)	χ^2	*P*-value	mOS (95% CI)	χ^2	*P*-value
CD3	Low	8.70 (7.10–11.80)	14.93	<0.001	16.40 (11.80–22.80)	10.92	0.001
	High	19.50 (14.20–26.20)			30.40 (25.20–43.70)		
CD4	Low	15.70 (11.20–20.20)	23.51	<0.001	15.70 (11.20–20.20)	12.80	<0.001
	High	38.90 (34.40–43.40)			31.70 (28.00–35.40)		
CD8	Low	9.70 (8.10–13.50)	16.52	<0.001	20.20 (14.70–26.00)	12.35	<0.001
	High	20.20 (12.90–30.10)			32.80 (23.40– 57.10)		
Foxp3	Low	15.00 (10.70–20.10)	2.47	0.116	27.00 (21.50– 38.50)	4.06	0.044
	High	10.90 (8.40–17.10)			20.10 (11.80–26.90)		
CD68	Low	16.30 (12.00–20.40)	4.53	0.033	29.60 (22.80–47.90)	5.81	0.016
	High	9.70 (8.40–12.90)			20.10 (14.20–26.20)		
CD66b	Low	15.70 (11.80–20.20)	12.74	<0.001	28.10 (22.90–38.80)	8.06	0.005
	High	6.10 (5.10– 9.60)			12.50 (8.60– 20.30)		

CI, confidence interval; mRFS, median recurrence-free survival time; mOS, median overall survival time; OS, overall survival; RFS, recurrence-free survival.

https://doi.org/10.3350/cmh.2024.0296

Table 3. Univariate Cox proportion hazards regression analysis for RFS and OS (n=359)

Characteristics		Recurrence-free survival			Overall survival		
		HR (95% CI)	χ^2	*P*-value	HR (95% CI)	χ^2	*P*-value
Age	Continues	1.00 (0.99 to 1.01)	0.27	0.605	1.01 (1.00 to 1.02)	1.83	1.76
Age, years	≤50	1 (referent)			1 (referent)		
	>50	1.06 (0.79 to 1.43)	0.16	0.687	1.29 (0.94 to 1.78)	2.48	0.116
Gender	Female	1 (referent)			1 (referent)		
	Male	1.17 (0.92 to 1.50)	1.64	0.200	1.07 (0.83 to 1.38)	0.30	0.583
HBsAg	Negative	1 (referent)			1 (referent)		
	Positive	1.02 (0.79 to 1.33)	0.03	0.871	0.72 (0.54 to 0.96)	5.03	0.025
AFP, ng/mL	≤20	1 (referent)			1 (referent)		
	>20	0.99 (0.68 to 1.43)	0.01	0.939	0.84 (0.56 to 1.25)	0.73	0.394
CA19-9, U/L	≤36	1 (referent)			1 (referent)		
	>36	1.51 (1.18 to 1.94)	10.61	0.001	1.90 (1.46 to 2.48)	23.37	<0.001
GGT, U/L	≤54	1 (referent)			1 (referent)		
	>54	1.63 (1.28 to 2.09)	15.71	<0.001	1.92 (1.48 to 2.48)	24.41	<0.001
Liver cirrhosis	No	1 (referent)			1 (referent)		
	Yes	1.02 (0.77 to 1.36)	0.02	0.880	0.83 (0.61 to 1.12)	1.46	0.227
Tumor size, cm	≤5	1 (referent)			1 (referent)		
	>5	1.59 (1.25 to 2.04)	13.99	<0.001	1.65 (1.27 to 2.14)	14.63	<0.001
Tumor number	Single	1 (referent)			1 (referent)		
	Multiple	2.36 (1.82 to 3.06)	44.63	<0.001	2.66 (2.04 to 3.47)	55.61	<0.001
LVI	No	1 (referent)			1 (referent)		
	Yes	1.25 (0.93 to 1.67)	2.19	0.139	1.48 (1.10 to 1.97)	6.91	0.009
Lymphatic metastasis	No	1 (referent)			1 (referent)		
	Yes	2.41 (1.77 to 3.29)	33.29	<0.001	2.70 (1.96 to 3.72)	39.57	<0.001
Tumor encapsulation	Complete	1 (referent)			1 (referent)		
	None	1.46 (1.03 to 2.05)	4.62	0.032	1.46 (1.01 to 2.11)	4.16	0.041
Tumor differentiation	I+II	1 (referent)			1 (referent)		
	III+IV	1.31 (1.03 to 1.67)	4.90	0.027	1.43 (1.11 to 1.84)	7.83	0.005
Tumor stage	I	1 (referent)			1 (referent)		
	II+III+IV	2.29 (1.79 to 2.93)	15.22	<0.001	2.78 (2.14 to 3.61)	63.58	<0.001
CD3	Low (≤142)	1 (referent)			1 (referent)		
	High (>142)	0.62 (0.49 to 0.79)	14.93	<0.001	0.66 (0.51 to 0.84)	10.92	0.001
CD4	Low (≤90)	1 (referent)			1 (referent)		
	High (>90)	0.59 (0.44 to 0.79)	11.42	<0.001	0.51 (0.38 to 0.67)	20.14	<0.001
CD8	Low (≤24)	1 (referent)			1 (referent)		
	High (>24)	0.61 (0.48 to 0.77)	16.52	<0.001	0.64 (0.49 to 0.82)	12.35	<0.001
Foxp3	Low (≤28)	1 (referent)			1 (referent)		
	High (>28)	1.23 (0.95 to 1.60)	2.47	0.116	1.32 (1.01 to 1.72)	4.06	0.044
CD68	Low (≤95)	1 (referent)			1 (referent)		
	High (>95)	1.30 (1.02 to 1.66)	4.53	0.033	1.36 (1.06 to 1.76)	5.81	0.016
CD66b	Low (≤600)	1 (referent)			1 (referent)		
	High (>600)	1.75 (1.28 to 2.39)	12.74	<0.001	1.59 (1.15 to 2.20)	8.06	0.005
Stroma	Dormant	1 (referent)			1 (referent)		
	Fibrogenic	1.67 (1.15 to 2.43)	7.41	0.007	1.81 (1.20 to 2.73)	8.16	0.004
	Inert	1.46 (1.00 to 2.14)	3.92	0.048	1.74 (1.15 to 2.64)	7.07	0.008
	Fibrolytic	2.35 (1.59 to 3.49)	19.16	<0.001	2.77 (1.81 to 4.22)	24.03	<0.001

CI, confidence interval; AFP, alpha-fetoprotein; GGT, gamma glutamyl transferase; CA 19-9, carbohydrate antigen 19-9; LVI, lymphatic vascular invasion.

with regard to the stromal types in a stratified survival analysis. CD3+, CD4+, and CD8+ cells predicted the prognosis for most stromal subtypes, whereas CD66b+ cells mainly predicted prognosis for fibrolytic stroma (Supplementary Table 3). Additionally, Foxp3+ cells could predict OS in patients with fibrogenic stroma (Supplementary Table 3). Taken collectively, the types of stroma not only differed in their expression of α-SMA and collagen-I but also displayed distinct patterns of immune cells, which were predictive of patient prognosis.

The contribution of stromal and immune markers to prognosis stratification

Because stromal and immune markers showed potential in stratifying patient prognosis, we performed a pairwise survival analysis of tumor-infiltrating leukocytes and stroma types with Bonferroni adjustment. Patients with high CD3, CD4, and CD8 expression and dormant stroma showed significantly better prognosis than other subgroups. Conversely, patients with low CD3, CD4, and CD8 expression and fibrolytic stroma showed significantly worse prognosis than other subgroups. Low Foxp3 expression with fibrolytic stroma also showed associations with prognosis compared with other subgroups. In addition, CD68 stratification had an association with prognosis. High CD66b expression with inert stroma showed significant associations with prognosis compared with low CD66b expression with dormant, fibrogenic, or inert stroma (Supplementary Fig. 1).

Lymphatic metastasis is a major factor that influences the

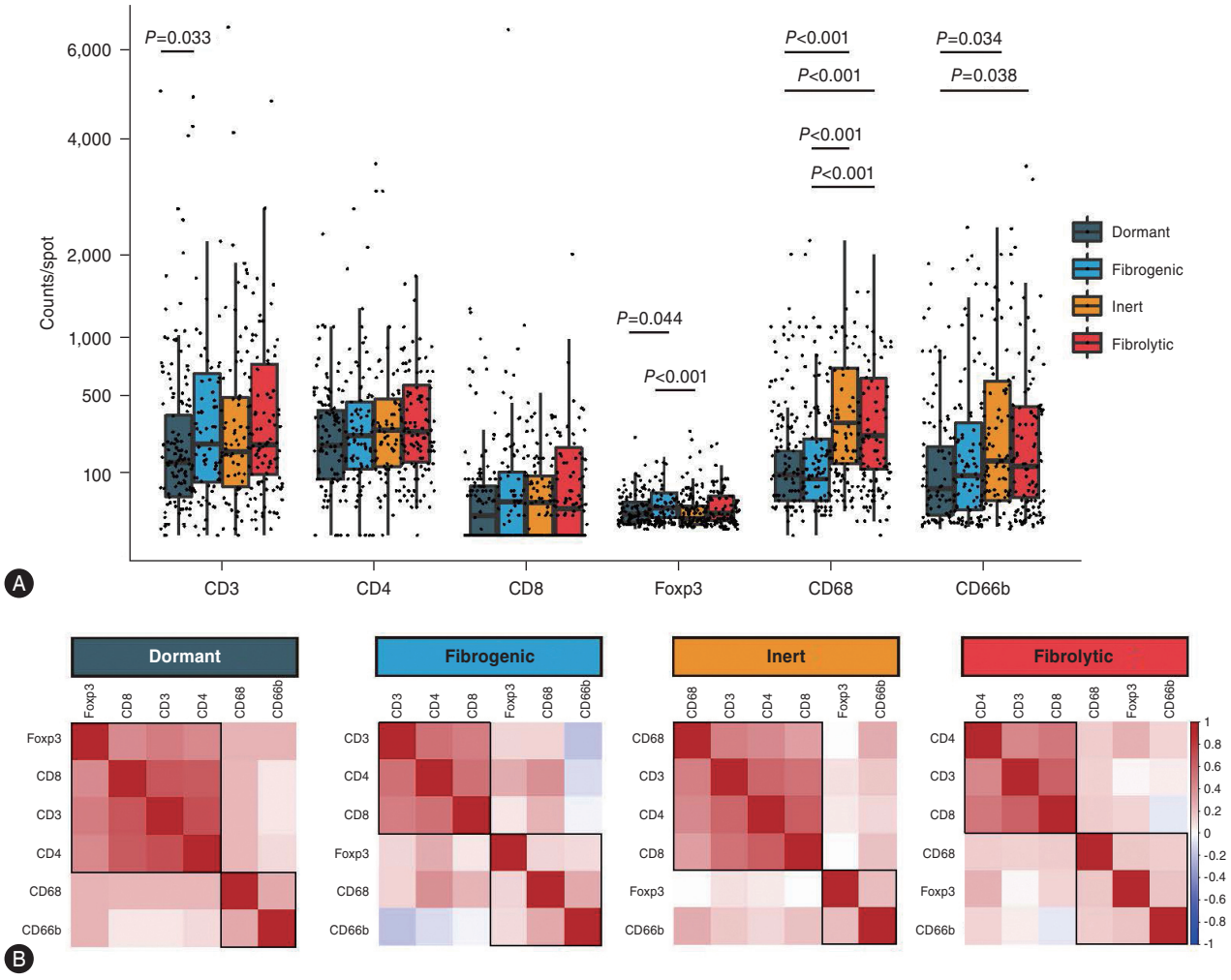

Figure 2. Interactive of tumor infiltrated leukocytes regarding different stromal types. (A) Distribution of different tumor infiltrated leukocytes in different stromal types. (B) Comparative correlation analysis of tumor infiltrated leukocytes in different stroma types.

https://doi.org/10.3350/cmh.2024.0296

prognosis of patients with ICC. Therefore, we asked whether the influence of tumor-infiltrating leukocytes and stroma type on prognosis was biased by lymphatic metastasis status. In patients with lymphatic metastasis, only dichotomization based on CD66b influenced prognosis, whereas dichotomization based on CD3, CD4, CD8, CD68, CD66b, and stroma type influenced prognosis in patients without lymphatic metastasis (Supplementary Tables 4, 5). Pairwise survival analysis solidified the results that lymphatic metastasis is an important prognostic factor, but tumor-in-

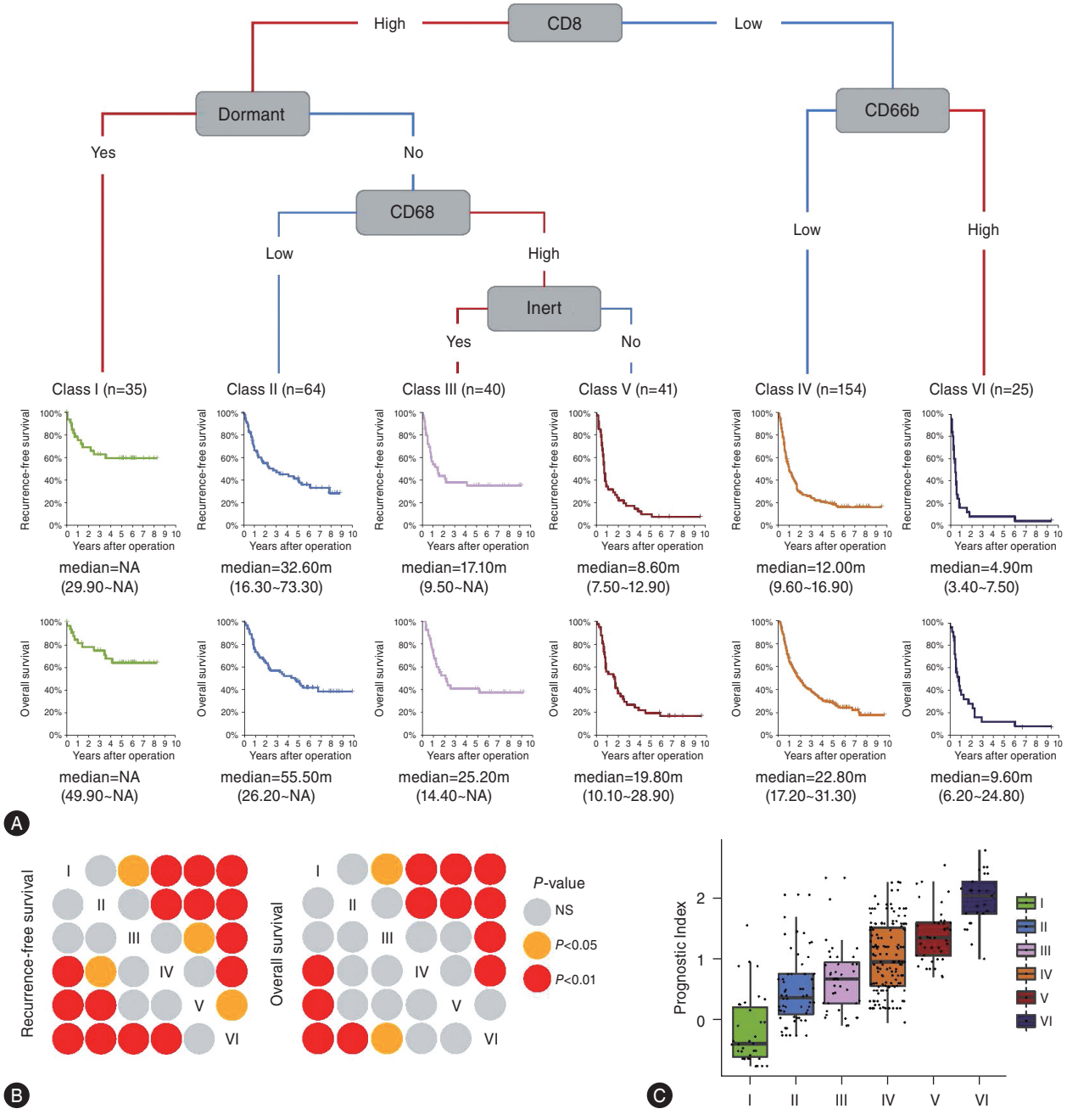

Figure 3. Integrating prognostic stromal-immune signature to predict recurrence-free survival. (A) Recursive partition survival tree defines the stromal-immune signature with separate median RFS and OS. (B) Pairwise survival analysis of stromal-immune signature with Bonferroni adjustment in left low triangle and none adjustment in right upper triangle for RFS and OS. (C) Boxplot illustrates the prognostic index by Cox multivariate model in different stromal-immune signature. RFS, recurrence-free survival; OS, overall survival.

https://doi.org/10.3350/cmh.2024.0296

filtrating leukocytes and stroma type also contribute to prognosis in patients without lymphatic metastasis (Supplementary Figs. 2 and 3).

Development of a stromal-immune signature to predict prognosis in ICC

We showed the prognostic values of stromal composition and immune cells and their interaction effects by hierarchy. To integrate the stromal composition and immune cells and evaluate their effects on ICC prognosis, we used the rpart algorithm, which could sort out several stromal-immune signatures. First, we used a nonparametric random survival forest approach and evaluated the importance of all tumor-infiltrating leukocytes and stroma types based on VIMP and MD to select variables to enroll into the model. The most important variable based on VIMP was CD66b, followed by CD3, stroma type, CD8, CD4, CD68, and Foxp3 (Supplementary Fig. 4A). The most important variable based on MD was stroma type, followed by CD66b, CD8, CD3, CD4, CD68, and Foxp3 (Supplementary Fig. 4B).

Consequently, all variables were enrolled into recursive partitioning for a discrete-time survival tree. We detected six terminal nodes and sorted out six classes, characterizing a unique stromal-immune signature with decreased median RFS and OS (Fig. 3A). Class I, characterized by dormant stroma and high CD8 expression, had the best prognosis with unreached median RFS and OS. Class VI,

Table 4. Multivariable Cox analysis of the stromal immune signature and clinicopathological characteristics for RFS and OS in validation cohort (n=240)

Characteristics		Recurrence-free survival			Overall survival		
		HR (95% CI)	z score	*P*-value	HR (95% CI)	z score	*P*-value
CA19-9, U/L	≤36	1 (referent)			1 (referent)		
	>36	1.14 (0.81 to 1.61)	0.776	0.438	1.11 (0.74 to 1.62)	0.479	0.632
GGT, U/L	≤54	1 (referent)			1 (referent)		
	>54	1.27 (0.90 to 1.80)	1.380	0.168	1.37 (0.93 to 2.03)	1.586	0.113
HBsAg	Negative	1 (referent)			1 (referent)		
	Positive	0.73 (0.52 to 1.03)	–1.790	0.073	0.68 (0.46 to 1.00)	–1.927	0.054
Tumor size, cm	≤5	1 (referent)			1 (referent)		
	>5	1.48 (1.05 to 2.09)	2.255	0.024	1.27 (0.85 to 1.89)	1.158	0.247
Tumor number	Single	1 (referent)			1 (referent)		
	Multiple	1.13 (0.61 to 2.09)	0.388	0.698	1.31 (0.67 to 2.55)	0.789	0.430
LVI	No	1 (referent)			1 (referent)		
	Yes	1.36 (0.73 to 2.53)	0.958	0.338	1.47 (0.75 to 2.89)	1.128	0.259
Lymphatic metastasis	No	1 (referent)			1 (referent)		
	Yes	1.90 (1.17 to 3.07)	2.615	0.009	2.33 (1.43 to 3.81)	3.377	<0.001
Tumor differentiation	I+II	1 (referent)			1 (referent)		
	III+IV	1.08 (0.77 to 1.52)	0.472	0.637	1.38 (0.94 to 2.02)	1.633	0.103
Tumor stage	I	1 (referent)			1 (referent)		
	II+III+IV	1.24 (0.57 to 2.66)	0.543	0.587	1.13 (0.49 to 2.64)	0.294	0.769
Class	I	1 (referent)			1 (referent)		
	II	1.65 (0.88 to 3.10)	1.555	0.120	1.70 (0.87 to 3.36)	1.542	0.123
	III	2.18 (1.10 to 4.30)	2.247	0.024	2.12 (1.03 to 4.40)	2.034	0.041
	IV	2.70 (1.51 to 4.84)	3.352	<0.001	2.41 (1.28 to 4.51)	2.738	0.006
	V	3.97 (2.10 to 7.52)	4.229	<0.001	3.35 (1.69 to 6.66)	3.449	<0.001
	VI	6.91 (3.47 to 13.79)	5.491	<0.001	5.12 (2.47 to 10.60)	4.394	<0.001

AFP, alpha-fetoprotein; GGT, gamma glutamyl transferase; CA 19-9, carbohydrate antigen 19-9; LVI, lymphatic vascular invasion; HR, hazard ratio.

https://doi.org/10.3350/cmh.2024.0296

characterized by low CD8 expression and high CD66b expression had the worst median RFS of 4.90 months (95% CI 3.40–7.50 months) and median OS of 9.6 months (95% CI 6.20–24.80 months; Fig. 3A). A paired survival analysis was conducted to compare each class (Fig. 3B). We applied a boxplot to illustrate the prognostic index (PI) in a Cox multivariable model for different stromal-immune signatures (Fig. 3C). The median PI increased from Class I to Class VI, indicating progressively poorer prognosis from Class I to Class VI.

We performed Chi-square tests to compare the clinicopathological characteristics of each class. We found that HBsAg, liver cirrhosis, tumor size, tumor number, and TNM stage were associated with the signature (Supplementary Table 6). Adjusted pairwise comparisons showed that Class III had higher rates of positive HBsAg and liver cirrhosis than Class IV, and Class VI showed more multiple tumors than Class V and higher TNM stage than Class I (Supplementary Fig. 5A–E).

Independent validation

To examine the predictive ability of the stromal-immune signature, we utilized a validation cohort of 240 patients and stained the stromal and immune markers of α-SMA, collagen, CD3, CD4, CD8, Foxp3, CD68, and CD66b. Patients with dormant stroma maintained the longest median RFS of 27.49 months (95% CI 23.21–31.77 months) and the longest median OS of 33.36 months (95% CI 29.52–37.20 months), whereas patients with fibrolytic stroma had the shortest median RFS of 12.20 months (95% CI 9.37–15.03 months) and shortest median OS of 21.05 months (95% CI 16.92–25.18 months; Supplementary Table 7 and Supplementary Fig. 6A). The results of univariate Cox proportion hazards regression analysis for RFS and OS in the validation cohort were similar to those in the training cohort (Supplementary Table 8).

We tested the stromal-immune signature in the validation cohort and observed results consistent with those in the test cohort. Class I displayed the best prognosis with median RFS of 28.07 months (95% CI 23.46–32.68 months) and median OS of 32.67 months (95% CI 28.27–37.07 months). Class VI had the worst prognosis with median RFS of 14.98 months (95% CI 9.61–20.34 months) and median OS of 18.93 months (95% CI 13.02–24.83 months; Supplementary Fig. 6B). Further results of multivariable Cox analysis of the stromal-immune signature for RFS and OS in the validation cohort confirmed that the signature was an independent risk factor (Table 4). In conclusion, the stromal-immune signature was robust in the validation cohort.

DISCUSSION

Several previous studies have shed light on the roles of stroma and infiltrating leukocytes in the tumor microenvironment.[16,17] However, their interaction as well as their prognostic values remained largely unknown considering the heterogeneities among patients and tumors. In this article, we demonstrated the clinical significance of stromal composition and immune cell infiltration in a large cohort of patients who received radical resection for ICC. To our knowledge, this is the first study in ICC that identified a prognostic signature of stromal composition and its association with immune cell infiltration and stratified patients with respect to prognosis. Our results suggest that patients who are predicted to have poor outcomes based on the stroma-immune signature need to be monitored especially closely after surgery.

ICC is a highly desmoplastic tumor with distinct stromal deposition. Our study confirmed the significance of α-SMA and collagen and their differential distributions in ICC. Patients with fibrolytic stroma characterized by high α-SMA and low collagen represent the subgroup with the lowest survival. CAFs exhibit high molecular and functional heterogeneity, which can either promote or constrain tumor growth.[18,19] CAFs positive for α-SMA expression promoted tumor cell proliferation and were indicators of poor prognosis in cancers of the hepatobiliary tract.[20,21] Type I collagen, the major component of fibrillar collagen during extracellular matrix deposition, can result in tumor stiffness.[22] Several studies showed that type I collagen inhibited tumor progression, possibly by its mechanical restriction.[19,23] These findings suggest that selectively targeting CAFs and conserving type I collagen might be an approach to inhibit ICC progression.

The contexture of tumor-infiltrating immune cells influences both prognosis and anti-cancer therapies. High densities of CD3+, CD4+, and CD8+ T cells were predictive of

favorable prognosis and response to therapies, whereas Foxp3+ regulatory T cells had the opposite effects.[15] Macrophage and neutrophil polarization represents a double-edged sword in anti-cancer immunity but tends to favor immunosuppressive effects more often than immune activation.[15,24] We confirmed the effects of these tumor-infiltrating immune cells and showed their joint effects with the stroma type. Immune cells, including CD3+, Foxp3+, CD68+, and CD66b+ cells, were differentially distributed with respect to stroma types, indicating the immune-heterogeneity of the stroma type. This heterogeneity might determine the effects of these immune cells in different stroma types. Levels of tumor-infiltrating CD3+, CD4+, and CD8+ T cells showed positive correlations with each other, and their dichotomization almost predicted RFS and OS in each stroma type. Hence, we considered that T cell immunity was of importance in ICC.

A fibro-inflammatory microenvironment influences ICC initiation, progression, and relapse.[7,25] Several studies indicated that the interplay and balance between CAFs and immune cells in cancer can determine the fate of the tumor. CAFs were able to induce an immune-suppressive environment, characterized by large inhibitory T-lymphocytes, myeloid-derived suppressor cells (MDSCs), and cytokine secretion.[22,26] These changes influence the function of CD8+ T cells and further impact immunotherapy.[27] CAFs recruit CD4+CD25+ T cells and mediate their trans-differentiation into CD4+CD25+Foxp3+ regulatory lymphocytes to inhibit CD4+ T cell proliferation.[28] CAFs also participate in TAM and TAN recruitment and phenotype polarization to tumor-promoting types.[29-33] Therefore, reforming the stroma to avert the immune-suppressive tumor environment might be a strategy to enhance tumor immunotherapy.

The stromal and immune components are sensitive to the microenvironment and change with the microenvironment as a reflection of tumor development.[34,35] In our study, we integrated the immune and stromal signatures to predict RFS and OS in surgically resected ICC for the first time. In the validation cohort, the integrated signature worked well. Common prognostic values in patients receiving resection are mainly based on clinical characteristics including tumor diameter, tumor number, lymph node metastasis, and lymphatic vascular invasion.[36] The stromal-immune signature was a supplement for the contemporary clinical prognostic models and helped better recognize patients with a high risk of recurrence and poor prognosis who need positive intervention. Considering the potential therapeutic role of therapies targeting CAFs and other immunotherapies,[37] the signature might even forecast the effects of these therapies, although this will require further validation. A recent study shed light on the heterogeneity of CAFs and the diverse immune profiles of the stroma in ICC.[38] The crosstalk between the stromal and immune components in the ICC tumor microenvironment was found to promote ICC growth and metastasis. For example, fibroblast activation protein (FAP), a serine protease that is selectively expressed on CAFs in many human solid tumors, was found to promote intrahepatic cholangiocarcinoma growth via MDSC recruitment.[39] Further studies of the mechanisms of the crosstalk and interaction between the stromal and immune components will help us to better understand the complexity of the ICC tumor microenvironment and how it is associated with patient outcomes.

ICCs display extensive intratumoral heterogeneity and exhibit spatiotemporally heterogeneous immunogenomic features across patients and within tumors.[40] Although our work delineates an integrated stromal-immune signature based on immune cell subpopulations and stromal composition to distinguish subgroups of patients with differences in RFS and OS, the results of TMA studies might be affected by the spatiotemporal heterogeneity of the ICC tumor microenvironment. Further study using single-cell profiling and high-resolution spatial omics will provide a greater and more comprehensive understanding of the ICC tumor microenvironment and enable further refinement of our conclusions.

Our study has certain limitations. First, our analyses and conclusions are limited by the single-center nature and further validation is warranted for clinical utility. Second, due to a tiny percentage of patients who received adjuvant treatment during 2009 to 2016, our study didn't reveal the role of stromal-immune signature in adjuvant treatment. With the advancement of ICC treatment, the number of ICC patients receiving adjuvant treatment after surgical resection is increasing. We will investigate whether our stromal-immune signature affects the efficacy of adjuvant treatment in a future study.

In conclusion, we defined a stromal-immune prognostic signature based on the tumor stromal composition and immune context to predict RFS and OS in patients with ICC.

https://doi.org/10.3350/cmh.2024.0296

The signature can help us better understand the reciprocal effects of tumor stroma and immune infiltration on ICC progression and outcomes.

Authors' contribution

YHY, HYX and JLL performed the experiments. SLZ analyzed the data. NL, SYP, LC and JYP provided the samples. ZQH, PCW, CBL and RQS provided critical thinking. YHY, HYX and SLZ wrote the paper. JF, ZJ and ZJZ commented on the study and revised the paper. SLZ obtained funding and designed the research.

Acknowledgements

This study was jointly supported by the National Natural Science Foundation of China (No. 82372985, No. 82373418, No. 82273247, No. 82173260, No. 82072681, No. 82003082), Shanghai Technical Standard Program (21DZ2201100) and Shanghai Medical Innovation Research Project (22Y11907300).

Conflicts of Interest

The authors have no conflicts to disclose.

SUPPLEMENTARY MATERIAL

Supplementary material is available at Clinical and Molecular Hepatology website (http://www.e-cmh.org).

REFERENCES

1. Banales JM, Cardinale V, Carpino G, Marzioni M, Andersen JB, Invernizzi P, et al. Expert consensus document: cholangiocarcinoma: current knowledge and future perspectives consensus statement from the European Network for the Study of Cholangiocarcinoma (ENS-CCA). Nat Rev Gastroenterol Hepatol 2016;13:261-280.
2. Mavros MN, Economopoulos KP, Alexiou VG, Pawlik TM. Treatment and prognosis for patients with intrahepatic cholangiocarcinoma: systematic review and meta-analysis. JAMA Surg 2014;149:565-574.
3. Sirica AE, Gores GJ, Groopman JD, Selaru FM, Strazzabosco M, Wei Wang X, et al. Intrahepatic cholangiocarcinoma: continuing challenges and translational advances. Hepatology 2019;69:1803-1815.
4. Tian MX, Zhou YF, Qu WF, Liu WR, Jin L, Jiang XF, et al. Histopathology-based immunoscore predicts recurrence for intrahepatic cholangiocarcinoma after hepatectomy. Cancer Immunol Immunother 2019;68:1369-1378.
5. Gentles AJ, Newman AM, Liu CL, Bratman SV, Feng W, Kim D, et al. The prognostic landscape of genes and infiltrating immune cells across human cancers. Nat Med 2015;21:938-945.
6. Fridman WH, Zitvogel L, Sautès-Fridman C, Kroemer G. The immune contexture in cancer prognosis and treatment. Nat Rev Clin Oncol 2017;14:717-734.
7. Sirica AE, Gores GJ. Desmoplastic stroma and cholangiocarcinoma: clinical implications and therapeutic targeting. Hepatology 2014;59:2397-2402.
8. Ilyas SI, Gores GJ. Pathogenesis, diagnosis, and management of cholangiocarcinoma. Gastroenterology 2013;145:1215-1229.
9. Mahajan UM, Langhoff E, Goni E, Costello E, Greenhalf W, Halloran C, et al. Immune cell and stromal signature associated with progression-free survival of patients with resected pancreatic ductal adenocarcinoma. Gastroenterology 2018;155:1625-1639.e2.
10. Zhou Z, Wang P, Sun R, Li J, Hu Z, Xin H, et al. Tumor-associated neutrophils and macrophages interaction contributes to intrahepatic cholangiocarcinoma progression by activating STAT3. J Immunother Cancer 2021;9:e001946.
11. Wittekind C. Pitfalls in the classification of liver tumors. Pathologe 2006;27:289-293.
12. Amin MB, Edge SB, Greene FL, Byrd DR, Brookland RK, Washington MK, et al. AJCC Cancer Staging Manual. 8th ed. New York: Springer, 2017.
13. Zhou ZJ, Dai Z, Zhou SL, Fu XT, Zhao YM, Shi YH, et al. Overexpression of HnRNP A1 promotes tumor invasion through regulating CD44v6 and indicates poor prognosis for hepatocellular carcinoma. Int J Cancer 2013;132:1080-1089.
14. Zhou SL, Dai Z, Zhou ZJ, Chen Q, Wang Z, Xiao YS, et al. CXCL5 contributes to tumor metastasis and recurrence of intrahepatic cholangiocarcinoma by recruiting infiltrative intratumoral neutrophils. Carcinogenesis 2014;35:597-605.
15. Camp RL, Dolled-Filhart M, Rimm DL. X-tile: a new bio-informatics tool for biomarker assessment and outcome-based cut-point optimization. Clin Cancer Res 2004;10:7252-7259.
16. Grivennikov SI, Greten FR, Karin M. Immunity, inflammation, and cancer. Cell 2010;140:883-899.
17. Fridman WH, Pagès F, Sautès-Fridman C, Galon J. The immune contexture in human tumours: impact on clinical out-

come. Nat Rev Cancer 2012;12:298-306.
18. Biffi G, Tuveson DA. Diversity and biology of cancer-associated fibroblasts. Physiol Rev 2021;101:147-176.
19. Özdemir BC, Pentcheva-Hoang T, Carstens JL, Zheng X, Wu CC, Simpson TR, et al. Depletion of carcinoma-associated fibroblasts and fibrosis induces immunosuppression and accelerates pancreas cancer with reduced survival. Cancer Cell 2014;25:719-734.
20. Okabe H, Beppu T, Hayashi H, Horino K, Masuda T, Komori H, et al. Hepatic stellate cells may relate to progression of intrahepatic cholangiocarcinoma. Ann Surg Oncol 2009;16:2555-2564.
21. Chuaysri C, Thuwajit P, Paupairoj A, Chau-In S, Suthiphongchai T, Thuwajit C. Alpha-smooth muscle actin-positive fibroblasts promote biliary cell proliferation and correlate with poor survival in cholangiocarcinoma. Oncol Rep 2009;21:957-969.
22. Yamauchi M, Barker TH, Gibbons DL, Kurie JM. The fibrotic tumor stroma. J Clin Invest 2018;128:16-25.
23. Bhattacharjee S, Hamberger F, Ravichandra A, Miller M, Nair A, Affo S, et al. Tumor restriction by type I collagen opposes tumor-promoting effects of cancer-associated fibroblasts. J Clin Invest 2021;131:e146987.
24. Jaillon S, Ponzetta A, Di Mitri D, Santoni A, Bonecchi R, Mantovani A. Neutrophil diversity and plasticity in tumour progression and therapy. Nat Rev Cancer 2020;20:485-503.
25. Sia D, Hoshida Y, Villanueva A, Roayaie S, Ferrer J, Tabak B, et al. Integrative molecular analysis of intrahepatic cholangiocarcinoma reveals 2 classes that have different outcomes. Gastroenterology 2013;144:829-840.
26. Mhaidly R, Mechta-Grigoriou F. Role of cancer-associated fibroblast subpopulations in immune infiltration, as a new means of treatment in cancer. Immunol Rev 2021;302:259-272.
27. Hegde PS, Chen DS. Top 10 challenges in cancer immunotherapy. Immunity 2020;52:17-35.
28. Costa A, Kieffer Y, Scholer-Dahirel A, Pelon F, Bourachot B, Cardon M, et al. Fibroblast heterogeneity and immunosuppressive environment in human breast cancer. Cancer Cell 2018;33:463-479.e10.
29. Gok Yavuz B, Gunaydin G, Gedik ME, Kosemehmetoglu K, Karakoc D, Ozgur F, et al. Cancer associated fibroblasts sculpt tumour microenvironment by recruiting monocytes and inducing immunosuppressive PD-1+ TAMs. Sci Rep 2019;9:3172.
30. Zhang R, Qi F, Zhao F, Li G, Shao S, Zhang X, et al. Cancer-associated fibroblasts enhance tumor-associated macrophages enrichment and suppress NK cells function in colorectal cancer. Cell Death Dis 2019;10:273.
31. Nagarsheth N, Wicha MS, Zou W. Chemokines in the cancer microenvironment and their relevance in cancer immunotherapy. Nat Rev Immunol 2017;17:559-572.
32. Liu T, Han C, Wang S, Fang P, Ma Z, Xu L, et al. Cancer-associated fibroblasts: an emerging target of anti-cancer immunotherapy. J Hematol Oncol 2019;12:86.
33. Song M, He J, Pan QZ, Yang J, Zhao J, Zhang YJ, et al. Cancer-associated fibroblast-mediated cellular crosstalk supports hepatocellular carcinoma progression. Hepatology 2021;73:1717-1735.
34. Binnewies M, Roberts EW, Kersten K, Chan V, Fearon DF, Merad M, et al. Understanding the tumor immune microenvironment (TIME) for effective therapy. Nat Med 2018;24:541-550.
35. Maynard A, McCoach CE, Rotow JK, Harris L, Haderk F, Kerr DL, et al. Therapy-induced evolution of human lung cancer revealed by single-cell RNA sequencing. Cell 2020;182:1232-1251.e22.
36. Hyder O, Marques H, Pulitano C, Marsh JW, Alexandrescu S, Bauer TW, et al. A nomogram to predict long-term survival after resection for intrahepatic cholangiocarcinoma: an Eastern and Western experience. JAMA Surg 2014;149:432-438.
37. Mao X, Xu J, Wang W, iang C, Hua J, Liu J, et al. Crosstalk between cancer-associated fibroblasts and immune cells in the tumor microenvironment: new findings and future perspectives. Mol Cancer 2021;20:131.
38. Zhang M, Yang H, Wan L, Wang Z, Wang H, Ge C, et al. Single-cell transcriptomic architecture and intercellular crosstalk of human intrahepatic cholangiocarcinoma. J Hepatol 2020;73:1118-1130.
39. Lin Y, Li B, Yang X, Cai Q, Liu W, Tian M, et al. Fibroblastic FAP promotes intrahepatic cholangiocarcinoma growth via MDSCs recruitment. Neoplasia 2019;21:1133-1142.
40. Lin Y, Peng L, Dong L, Liu D, Ma J, Lin J, et al. Geospatial immune heterogeneity reflects the diverse tumor-immune interactions in intrahepatic cholangiocarcinoma. Cancer Discov 2022;12:2350-2371.